The Mars Exploration Rover Instrument Positioning System

Eric T. Baumgartner, Robert G. Bonitz, Lori R. Shiraishi, Joseph P. Melko and P. Chris Leger
Jet Propulsion Laboratory
4800 Oak Grove Drive
Pasadena, CA 91109-8099
Eric.T.Baumgartner,Robert.G.Bonitz,Lori.R.Shiraishi,Joseph.P.Melko,Chris.Leger@jpl.nasa.gov

Abstract—During Mars Exploration Rover (MER) surface operations, the scientific data gathered by the *in situ* instrument suite has been invaluable with respect to the discovery of a significant water history at Meridiani Planum and the hint of water processes at work in Gusev Crater. Specifically, the ability to perform precision manipulation from a mobile platform (i.e., mobile manipulation) has been a critical part of the successful operation of Spirit and Opportunity rovers. As such, this paper describes the MER Instrument Positioning System that allows the *in situ* instruments to operate and collect their important science data using a robust, dexterous robotic arm combined with visual target selection and autonomous software functions.

TABLE OF CONTENTS

1.INTRODUCTION 1
2.DRIVING SYSTEM REQUIREMENTS 2
3.ALGORITHMS AND SOFTWARE 3
4.SUB-SYSTEM CALIBRATION 9
5.SURFACE OPERATIONS HIGHLIGHTS 12
6.CONCLUSIONS 12
REFERENCES 13
BIOGRAPHY 13

1. INTRODUCTION

The Mars Exploration Rovers, Spirit and Opportunity, carry a unique *in situ* instrument suite that has been designed to measure and understand the detailed geochemistry and morphology of the surface of Mars [1]. The *in situ* instrument suite includes the Möessbauer Spectrometer (MB) [2], the Alpha Particle X-ray Spectrometer (APXS) [3], the Microscopic Imager (MI) [4] and the Rock Abrasion Tool (RAT) [5]. The deployment and placement of these instruments onto the Martian surface (both soil and rock targets) is controlled by the 5 degree-of-freedom Instrument Deployment Device (IDD). The IDD represents the most dexterous robotic manipulator ever flown to another lunar or planetary surface.

The IDD is mounted towards the front of the rover and is capable of reaching out approximately 0.75 meters in front of the rover at full extent. The IDD weighs approximately 4 kg and carries a 2 kg payload mass (instruments and associated structure). The design of the mechanical aspects of the IDD is described in [6]. During rover driving activities, the IDD is contained within a stowed volume that does not impact the rover's ability to traverse safely across the Martian terrain. The location of soil and rock targets which the scientists select for instrument placement activities are specified using the front Hazard avoidance cameras (or front Hazcams) which are configured as a stereo camera pair.

On-board software controls the IDD based on sequences developed by ground operators. The on-board software contains numerous low-level and high-level functions for controlling the IDD such as actuator current limiting based on temperature and pose, inverse kinematic Cartesian control, deflection compensation due to gravity and tilt-induced droop, model-based pre-loading fo instruments on hard targets, instrument placement using proximity feedback sensors, etc. For the MER project, the entire scope of work associated with the design, development, test and operation of the IDD and in situ instruments was grouped into the Instrument Positioning System. As with many of the other rover sub-systems, the IPS was a collaborative effort between scientists, engineers, and instrument developers that culminated in the successful operation of this dexterous robot arm for collecting important science data.

This paper will first lay out a summary of the system requirements that drove the design of the overall IPS. The paper will also detail the flight software functions and algorithms utilized to command and control the IDD in order to perform autonomous surface operations. The IPS test program will also be described including the results from sub-system calibration activities. Finally, specific results and experiences from the surface operations phase will be presented, in particular, those results that highlight

0-7803-8155-6/04/$17.00©2004 IEEE

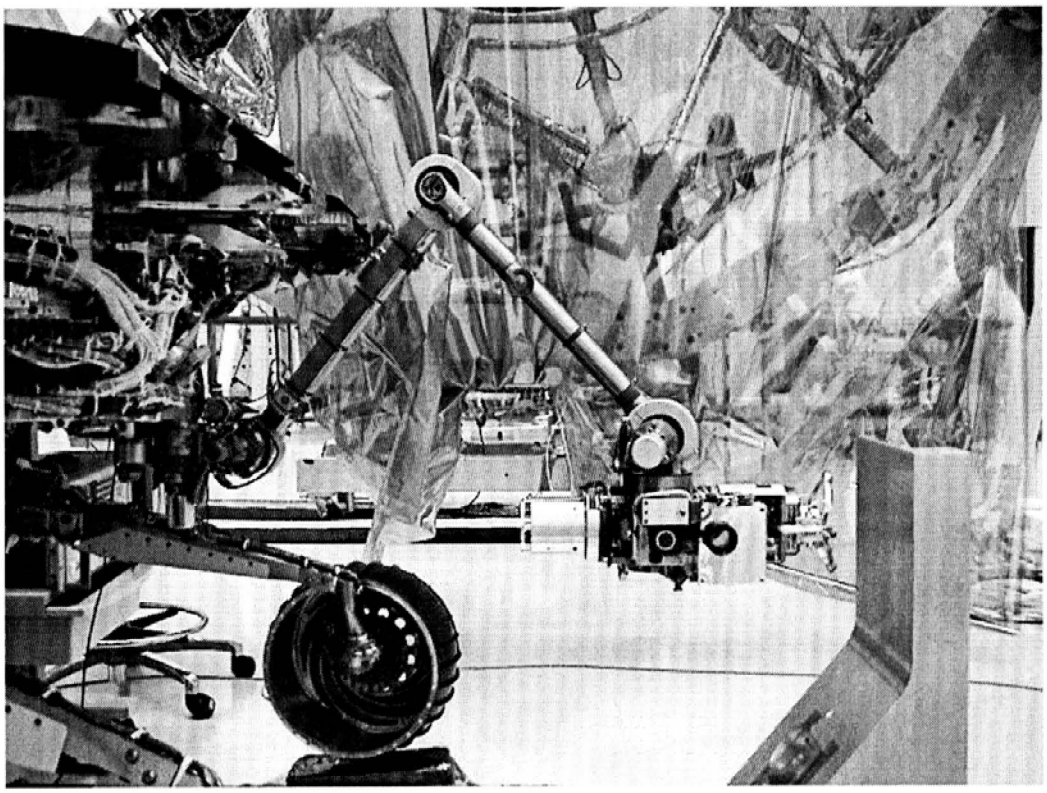

Figure 1: MER Instrument Positioning System

the precision and robustness of this robotic instrument positioning system.

2. DRIVING SYSTEM REQUIREMENTS

The MER Instrument Positioning System (IPS) is shown in Figure 1. The IPS includes the 5 degree-of-freedom robotic arm known as the Instrument Deployment Device (IDD) that is utilized to place and hold the in situ instruments on rock and soil targets located within the IDD work volume and the rover-mounted targets such as the dust collecting magnets and instrument calibration targets. For placement of the instruments on rock and soil targets, a wide field-of-view stereo imaging system known as the front Hazcams are used to specify the 3D location and surface normal of the target with respect to the rover's coordinate frame. On-board software is then used to drive the IDD so that the selected instrument achieves the desired 3D position and 2D orientation (azimuth and elevation) relative to the target of interest. Proximity sensors are located on all instruments so that contact with the target surface can be detected and trigger the termination of the IDD movement.

The driving system requirements for the IPS are primarily concerned with the absolute and relative positioning performance associated with the placement of the instruments on targets of interest including rock and soil targets as well as rover-mounted targets. The absolute positioning requirement stated that the IPS shall be capable of positioning each *in situ* payload element to within 10 mm in position and 10 degrees with respect to the surface normal of a science target that has not been previously contacted by another *in situ* instrument. This requirement was then broken down into two error budgets associated with the ability of the IDD to achieve a certain instrument position and orientation and the ability of the front Hazcam stereo camera pair to resolve the 3D position and surface normal of a science target. Therefore, the overall absolute positioning error requirement was split equally into two error budgets.

The IDD was required to be capable of achieving a position accuracy of 5 mm and an angular accuracy of 5 degrees in free space within the dexterous workspace of the IDD. Factors that affect the ability of the IDD to meet this requirement include knowledge of the IDD kinematics (link lengths, link offsets, etc), knowledge of the location of actuator hardstops, actuator backlash effects, actuator closed-loop controller resolution, and knowledge of IDD stiffness parameters. A calibration procedure (to be described in Section 5) was utilized to experimentally determine the parameters that affect the IDD positioning performance. The remaining half of the error budget was assigned to the front Hazcam stereo pair such that the vision system was required to determine the location of the science

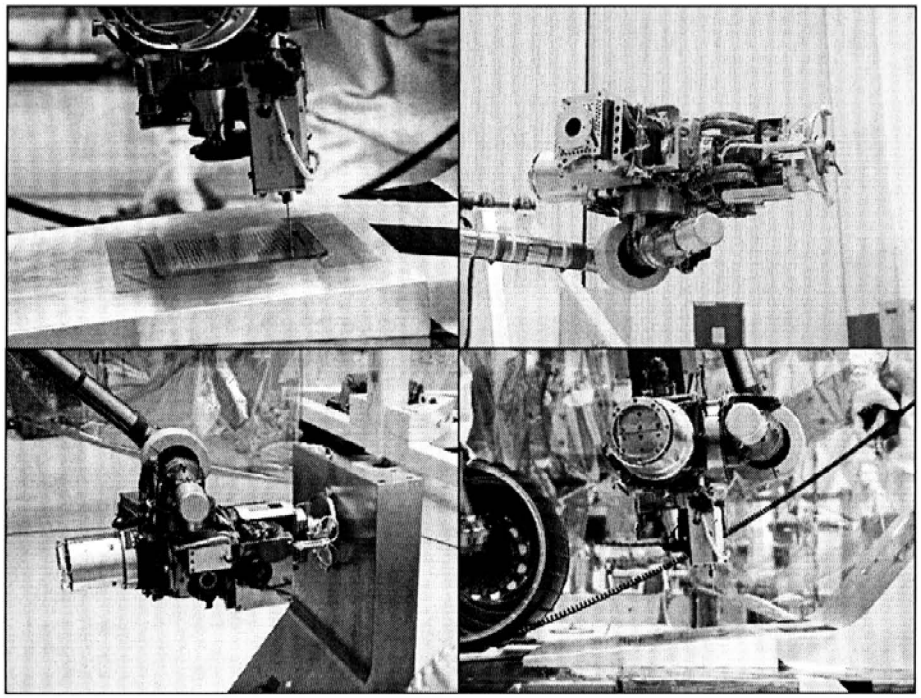

Figure 2: Instrument Proximity Sensors

target with a position accuracy of 5 mm and the angular accuracy was 5 degrees with respect to the target's surface normal. The factors that affect the ability of the stereo camera pair to meet this requirement include camera calibration errors, stereo correlation errors, and image resolution issues.

Another driving system requirement is associated the repeatability of the IDD in terms of being able to place one instrument on a science target after the target has been contacted by a different instrument, to place the instruments on rover-mounted targets, and to perform close-clearance operations such as stowing the IDD within its stowed position. The requirement specified that the repeatability of the IDD shall be 4 mm in position and 3 mm in orientation. The final positioning requirement is associated with the ability of the IDD to incrementally position the MI. The MI is a fixed focus instrument with a depth of field of 3 mm. Therefore, the IDD serves as the focus mechanism for the MI. As such, the IDD is required to have a minimum controllable motion of 2 mm ± 1 mm.

In addition to the positioning requirements mentioned above, other driving system requirements included the ability to place any *in situ* instrument on a reachable science target within one command cycle and to be able to remove an instrument from a target and place a second instrument on the same target any time during the Martian diurnal cycle (i.e., day or night). For RAT grinding operations, the IDD is required to place and hold the RAT on the rock target with a specified pre-load. The IDD is required to provide the RAT with a pre-load of at least 10N within 90% of the reachable science target workspace. As mentioned previously, each instrument carried proximity sensors to detect contact between the instrument and the target surface. For the MI, MB and RAT, the contact sensors are configured to be dual redundant per instrument. The APXS instrument includes an integral dust door mechanism whose operation is controlled by the IDD's placement of the APXS on a hard target (rover-mounted target or a rock target). The APXS dust door mechanism includes a latch switch that is used to sense the successful opening or closing of the dust door and a second (non-redundant) contact switch that is activated after the dust door has been latched open. The proximity sensing devices for each *in situ* instrument are shown in Figure 2.

3. ALGORITHMS AND SOFTWARE

Overview

Control of the IDD is accomplished through a distributed architecture with the necessary functions implemented in various hardware and flight software (FSW) modules as depicted in Figure 3. Low-level PID control of the IDD motors and generation of trapezoidal velocity profiles are implemented in hardware on the Motor Control Board (MCB) using feedback from quadrature encoders on the motor shafts. The motor controller runs at a sampling frequency of 1KHz. The states of the joint potentiometers, temperature sensors, and contact switches (CSWs) are scanned by the Payload Services Analog Board (PSAB) and

converted to digital format for processing by the flight software. The states of the contact switches are also fed directly to the hardware motor controller so that motion can be terminated if so desired upon change of a switch state.

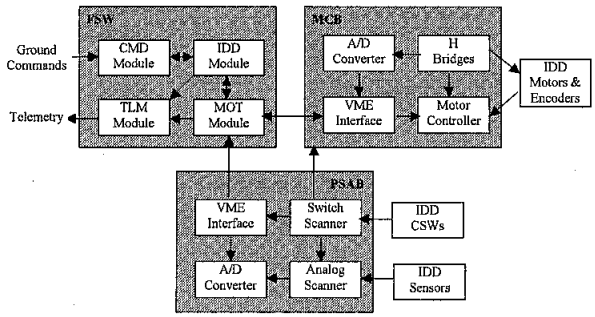

Figure 3: IDD Control Architecture

The FSW resides on the Command and Data Handling (C&DH) computer (a RAD6000) located in a VME chassis within the rover's electronics box. The FSW runs under VxWorks[1], a real-time multi-tasking operating system with selectable task priorities and preemptive rescheduling. The primary method of communication between tasks is via message passing. A high-level view of the IDD software module is depicted in Figure 4. The IDD task waits until a message is received and then responds to the message. After completing the response, it waits for the next message. The message can be a command, and out-of-bounds (OOB) message (e.g., stop), or a reply from the motor software containing the state of the IDD motors and sensors.

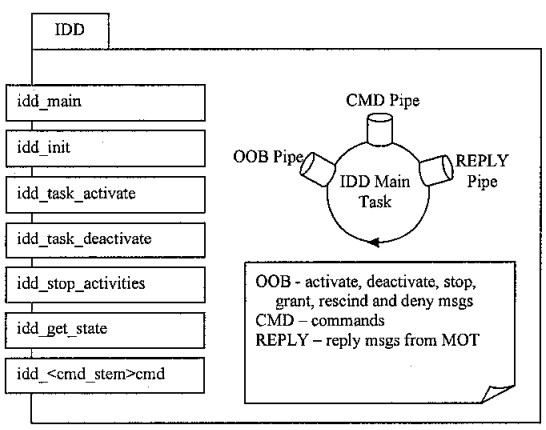

Figure 4: IDD Software Overview

The IDD software also provides a function for other software modules to get the IDD state information for inclusion in instrument (APXS, MB, MI, RAT) data products to make correlation of IDD state with the science data easy to do during ground data processing.

[1] VxWorks is registered trademark of Wind River Systems, Inc., 1010, Atlantic Avenue, Alameda, CA 94501

A simplified view of the sequence of events when the IDD software receives a command is depicted in Figure 5. Prior to actually moving the arm the IDD must get permission from the Activity Constraint Manager (ACM) and the Arbiter (ARB) to assure that it is safe to move the arm (e.g., not driving, no faults) and that the necessary resources are available (the motor controller is shared with other rover mechanisms). At the completion of the move, the resources are released and the IDD FSW replies to the command object that the command completed – successfully or not.

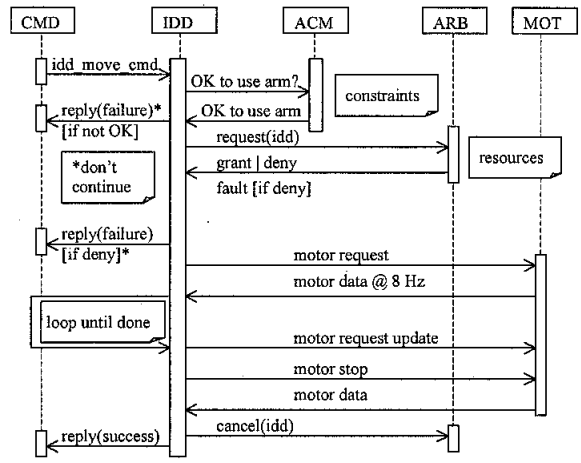

Figure 5: IDD Command Sequence Diagram

Kinematics

The IDD kinematics are defined using the Denavit-Hartenberg [7] representation with the coordinate frames assigned as shown in Figure 6 and summarized in Table 1. The z axis for each instrument frame is aligned with its "boresight." To eliminate joint angles that are congruent modulo 2π, each is uniquely expressed as a negative number from the joint's negative hardstop, $\theta_{\min_i}$, to zero and as a positive number from zero to the joint's positive hardstop, $\theta_{\max_i}$. The following link and joint parameters are defined:

a_i = i^{th} link length = distance along x_i from the intersection of the x_i and z_{i-1} axes to the origin of the ith frame;

d_i = i^{th} offset = distance along z_{i-1} from origin$_{i-1}$ to the intersection of the x_i and z_{i-1} axes;

ϕ_i = i^{th} twist = angle from z_{i-1} to z_i about x_i;

θ_i = i^{th} joint variable; the angle from x_{i-1} to x_i about z_{i-1}.

Link	a_i	α_i	d_i	θ_i
1	a_1	$\pi/2$	d_1	θ_1
2	a_2	0	0	θ_2
3	a_3	0	0	θ_3
4	0	$-\pi/2$	d_4	θ_4
5	0	$\pi/2$	d_5	θ_5

Table 1: IDD Kinematic Parameters

The following kinematic variables are defined:

Pose = [position orientation] - the Cartesian position and orientation of the designated instrument or tool frame (MB, APXS, RAT, MI) in the rover coordinate frame. Tool frames are located at the face of the instrument with the approach vector (z axis) along the "boresight."

Position - the x, y, and z coordinates of the origin of the tool frame in the rover frame.

Orientation - the direction of the tool frame approach vector (z axis) as specified by the azimuth and elevation angles, θ_{az} and θ_{el}. Since the IDD has only 5 DOF, the orientation about the approach vector is not controlled.

θ_{az} - the angle from the rover $+x$ axis to the projection of the tool approach vector onto the rover x-y plane with the positive sense being about the rover $+z$ axis using the right-hand rule. The rover $+x$ axis points forward and the $+z$ axis point down.

θ_{el} - the angle from the projection of the tool approach vector onto the rover x-y plane to the approach vector with the positive sense having the approach vector z coordinate greater than 0 for a positive angle.

Configuration – the geometric state of the shoulder, elbow and wrist. The shoulder can take on two values – RIGHT (1) or LEFT (-1), the elbow two values – UP (1) or DOWN (-1), and the wrist two values – UP (1) or DOWN (-1).

$${}^iT_j = \begin{bmatrix} {}^iR_j & {}^ip_j \\ 0\,0\,0 & 1 \end{bmatrix}$$ - the homogeneous transformation from frame i to j;

$${}^iR_j = \left[{}^in_j \;\; {}^is_j \;\; {}^ia_j \right]$$ - the orientation of frame j in frame i;

${}^ia_j$ - the unit vector of the z axis of frame j in frame i;

${}^ip_j$ - the vector from the origin of frame i to the origin of frame j.

Symbols used in the kinematic equations are:

$s_i = \sin(\theta_i)$;
$c_i = \cos(\theta_i)$;
$s_{ijk} = \sin(\theta_i + \theta_j + \theta_k)$;
$c_{ijk} = \cos(\theta_i + \theta_j + \theta_k)$.

The pose is computed from the joint angles by first computing the homogeneous transformation from the rover frame to the tool frame:

$${}^{rover}T_{tool} = {}^{rover}T_{IDDmnt}\,{}^{IDDmnt}T_{IDD0}\,{}^{IDD0}T_{IDD5}\,{}^{IDD5}T_{tool}$$

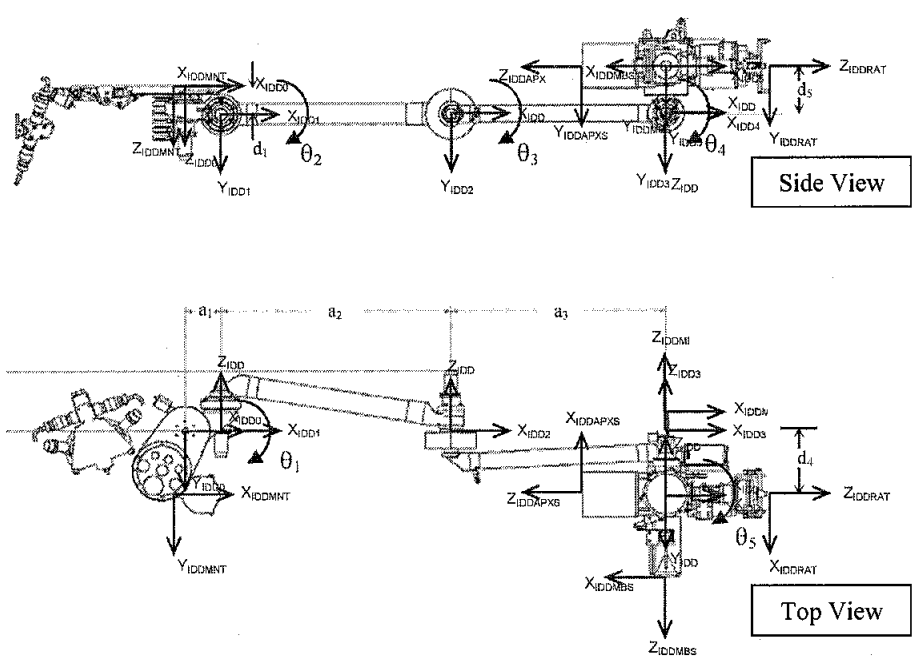

Figure 6: IDD Mechanical Layout and Coordinate Frame Conventions

where

$$
{}^{IDD0}T_{IDD5} = \begin{bmatrix} c_1c_{234}c_5 - s_1s_5 & -c_1s_{234} & c_1c_{234}s_5 + s_1c_5 & a_1c_1 + a_2c_1c_2 + a_3c_1c_{23} + d_4s_1 - d_5c_1s_{234} \\ s_1c_{234}c_5 + c_1s_5 & -s_1s_{234} & s_1c_{234}s_5 - c_1c_5 & a_1s_1 + a_2s_1c_2 + a_3s_1c_{23} - d_4c_1 - d_5s_1s_{234} \\ s_{234}c_5 & c_{234} & s_{234}s_5 & d_1 + a_2s_2 + a_3s_{23} + d_5c_{234} \\ 0 & 0 & 0 & 1 \end{bmatrix}
$$

and

$$
{}^{IDD5}T_{IDDtool} = \begin{bmatrix} c_{tool} & 0 & s_{tool} & {}^{5}p_{toolx} \\ 0 & 1 & 0 & 0 \\ -s_{tool} & 0 & c_{tool} & {}^{5}p_{toolz} \\ 0 & 0 & 0 & 1 \end{bmatrix}
$$

and then computing the pose from:

$$
pose = \left[{}^{rover}p_{tool}^{T} \quad a\tan 2\left({}^{rover}a_{tooly}, {}^{rover}a_{toolx}\right) \quad a\tan 2\left({}^{rover}a_{toolz}, \sqrt{{}^{rover}a_{tooly}^2 + {}^{rover}a_{toolx}^2}\right) \right]^T
$$

The configuration of the IDD is computed from:

$$
shoulder = \begin{cases} RIGHT & ;\ c_1\,{}^{IDD0}p_{IDD5x} + s_1\,{}^{IDD0}p_{IDD5y} \geq 0 \\ LEFT & ;\ c_1\,{}^{IDD0}p_{IDD5x} + s_1\,{}^{IDD0}p_{IDD5y} < 0 \end{cases}
$$

$$
elbow = \begin{cases} UP & ;\ shoulder = RIGHT\ \&\ {}^{IDD2}p_{IDD3y} \geq 0 \\ & ;\ shoulder = LEFT\ \&\ {}^{IDD2}p_{IDD3y} \leq 0 \\ DOWN & ;\ shoulder = RIGHT\ \&\ {}^{IDD2}p_{IDD3y} < 0 \\ & ;\ shoulder = LEFT\ \&\ {}^{IDD2}p_{IDD3y} > 0 \end{cases}
$$

$$
wrist = \begin{cases} UP & ;\ {}^{IDD0}a_{4z} \geq 0 \\ DOWN & ;\ {}^{IDD0}a_{4z} < 0 \end{cases}.
$$

The inverse kinematics was derived using geometric techniques and is computed as follows:

First compute the approach vector in the rover frame from the desired instrument azimuth and elevation angles:

$$
{}^{rover}a_{tool} = \left[c_{el}c_{az} \quad c_{el}s_{az} \quad s_{el} \right]^T.
$$

Compute the position of the turret frame in the IDD base frame:

$$
{}^{IDD0}p_{IDD5} = {}^{IDD0}p_{tool} - {}^{IDD0}a_{tool} \left\| {}^{5}p_{tool} \right\|.
$$

Then compute the joint angles:

$$
\theta_1 = \begin{cases} \alpha_1 + \beta_1 & ;\ shoulder = RIGHT \\ \alpha_1 - \beta_1 - \pi & ;\ shoulder = LEFT \end{cases}
$$

where

$$
\alpha_1 = a\tan 2\left({}^{IDD0}p_{IDD5y}, {}^{IDD0}p_{IDD5x}\right)
$$

$$
\beta_1 = a\tan 2\left(d_4, \sqrt{{}^{IDD0}p_{IDD5x}^2 + {}^{IDD0}p_{IDD\%y}^2 - d_4^2}\right)
$$

$$
\theta_2 = \alpha_2 - shoulder \times elbow \times \beta_2
$$

where

$$
\alpha_2 = a\tan 2\left({}^{IDD1}p_{IDD4y}, {}^{IDD1}p_{IDD4x}\right)
$$

$$
r_3 = \sqrt{{}^{IDD1}p_{IDD4x}^2 + {}^{IDD1}p_{IDD4y}^2}
$$

$$
\beta_2 = a\cos\left(\frac{r_3^2 + a_2^2 - a_3^2}{2r_3a_2}\right)
$$

$$
\theta_3 = a\tan 2\left(shoulder \times elbow \times s_3, c_3\right)
$$

where

$$
c_3 = \frac{r_3^2 - a_2^2 - a_3^2}{2a_2a_3}
$$

$$
s_3 = \sqrt{1 - c_3^2}
$$

$$
\theta_4 = \theta_{234} - \theta_2 - \theta_3
$$

where

$$
\theta_{234} = a\tan 2\left({}^{IDD0}a_{toolz}, c_1\,{}^{IDD0}a_{toolx} + s_1\,{}^{IDD0}a_{tooly}\right)
$$

$$
\theta_5 = a\tan 2\left(\begin{matrix} c_1c_{234}\,{}^{IDD0}a_{toolx} + s_1c_{234}\,{}^{IDD0}a_{tooly} + s_{234}\,{}^{IDD0}a_{toolz}, \\ s_1\,{}^{IDD0}a_{toolx} - c_1\,{}^{IDD0}a_{tooly} \end{matrix} \right) - \theta_{tool}
$$

Cartesian Trajectory Generation

When the IDD receives a Cartesian move command, a sequence of intermediate or via points between the starting and ending poses is generated prior to the initiation of motion. The number of via points generated satisfies the following conditions: 1) the deviation from the Cartesian straight-line path is less than the specified error bound, ε_p, and 2) the Cartesian distance between via points is less the specified allowable distance, δ_p. The concept is illustrated in Figure 7. A corresponding set of conditions is also satisfied for orientation with the error bound and distance designated as, ε_o, and δ_o, respectively. Finally, the distance in joint space between the via points must be less than the specified allowable distance, δ_q. The distance and error bounds will be stored in the parameter table and can be changed by the operator, but a hard-coded lower limit shall be enforced under which the operator cannot set the limits.

The change in orientation from the starting to ending poses is represented as a change in the azimuth and elevation angles, θ_{az} and θ_{el}. Since θ_{az} and θ_{el} uniquely determine the approach vector of the designated tool, the change in orientation from the starting to ending poses can also be represented by a change in the starting and ending approach vectors. The ending approach vector can be obtained by rotating the starting approach vector about the common normal between the starting and ending approach vectors by an angle, θ_{n_c}. The "straight-line" orientation path is defined as a linear interpolation of θ_{n_c} about the common normal

and is used in the generation of the via sequence.

The via sequence is generated using a recursive bisection method and converted to a joint via sequence using the inverse kinematics described above for each of the Cartesian via points. Prior to initiation of motion, each via point is checked for joint limit violations and collisions with the rover. Trapezoidal velocity profiles are generated in hardware on the MCB such that all joints arrive at their via points simultaneously. The IDD FSW processes the position data during motion at an 8 Hz rate and when the arm is close to reaching a via point, the registers in the MCB are updated to the next set of joint via points. The hardware velocity profiler automatically generates the trapezoidal profile to the next via point on the fly so that smooth motion through each via point is achieved.

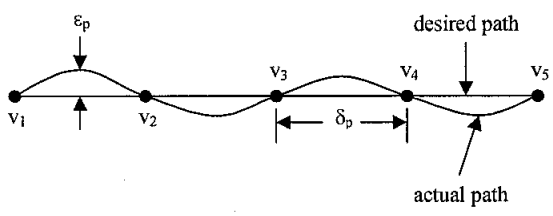

Figure 7: Cartesian Path Via Sequence

Deflection Compensation

The computation of the pose of the end effector from the joint angles using the forward kinematics function assumes that the IDD is rigid (i.e., infinitely stiff). However, the IDD's stiffness and mass properties are such that the endpoint can deflect significantly from the computed pose due to gravity. The deflection is also dependent on the tilt of the rover that affects the direction of the gravity vector relative to the IDD. In order to achieve the required placement accuracy, the commanded pose is adjusted based on the computed deflection. It is the adjusted pose that is used as the ending pose in the generation of the Cartesian via sequence described above. The computation is based on the stiffness model of the IDD and the mass properties of it and the instruments on the end effector. The deflection is dependent on the force exerted on the end effector and is used to compute the pose required to achieve a specified preload force on an instrument (e.g., RAT) when placed on a hard target.

The following parameters are defined for the deflection compensation algorithm:

m_i = lumped mass for the ith link (all elements between ith-1 frame and the ith frame)

${}^{i-1}p_{cm_i}$ = vector from the ith-1 coordinate frame to the ith center of mass when θ_i is zero

$K_i = \begin{bmatrix} k_{ix} & 0 & 0 \\ 0 & k_{iy} & 0 \\ 0 & 0 & k_{iz} \end{bmatrix}$ = torsional stiffness matrix at the ith frame

a_g = acceleration due to gravity.

The following variables are used in the algorithm:

${}^{i-1}R_{cm_i} = \begin{bmatrix} c_i & -s_i & 0 \\ s_i & c_i & 0 \\ 0 & 0 & 1 \end{bmatrix}$ = matrix representing rotation about the ith joint axis

${}^{i-1}T_{cm_i} = \begin{bmatrix} {}^{i-1}R_{cm_i} & {}^{i-1}R_{cm_i}\,{}^{i-1}p_{cm_i} \\ 0\ 0\ 0 & 1 \end{bmatrix}$ = homogeneous transformation from ith-1 frame to the ith center of mass

g_i = unit gravity vector at the ith center of mass in the ith center of mass frame

f_{end} = the force exerted along the tool frame z axis (approach vector)

$F_i = \begin{bmatrix} f_i^T & \tau_i^T \end{bmatrix}^T$ = the force and moment at the ith frame in ith frame coordinates

$\hat{p} = p\times = \begin{bmatrix} 0 & -p_z & p_y \\ p_z & 0 & -p_x \\ -p_y & p_x & 0 \end{bmatrix}$ = skew-symmetric cross-product operator for $p \in R^3$

${}^iAd_j = \begin{bmatrix} {}^iR_j & {}^i\hat{p}_j\,{}^iR_j \\ 0_3 & {}^iR_j \end{bmatrix}$ = adjoint transformation which transforms twists from the ith frame to the jth frame where 0_3 is the 3x3 zero matrix

${}^iAd_j^T = \begin{bmatrix} {}^iR_j^T & 0_3 \\ -{}^iR_j^T\,{}^i\hat{p}_j & {}^iR_j^T \end{bmatrix}$ = transpose of the adjoint transformation which transforms the force and moment acting at the ith frame to the force and moment acting at the jth frame.

Given the joint angles, the tilt, and the force exerted by the end effector, the deflected pose is computed as follows:

1. Compute the homogeneous transformations from the rover frame to the tool frame forward kinematics;
2. Compute the ith gravity vector:
   g_{rvr} = gravity vector in the rover frame
   for i = 1 to 5:
   $g_i = {}^{i-1}R_{cm_i}^T\,{}^{rvr}R_{i-1}^T g_{rvr}$;

3. Compute the force and moment vectors at ith frame:
$F_6 = F_{tool} = [0\ 0\ -f_{end}\ 0\ 0\ 0]^T$
for i = 5 to 0:
$$F_i = {}^{i+1}Ad_i^T F_{i+1} + {}^{cm_i}Ad_i^T [m_i a_g g_i^T\ 0\ 0\ 0]^T;$$
4. Compute the deflection and corresponding rotation matrix at the ith frame:
for i = 0 to 4:
$$d_i = {}^iR_{cm_i}^T K_i^{-1}\, {}^iR_{cm_i} \tau_i$$
${}^iR_d = aa2r(d_i, \|d_i\|)$ where *aa2r* transforms the axis-angle representation of the deflection to a rotation matrix in *SO(3)*;
5. Compute the ith deflected homogeneous transformation:
for i = 0 to 4:
$${}^iT_{i+1} = \begin{bmatrix} {}^iR_d\, {}^iR_{i+1} & {}^iR_d\, {}^ip_{i+1} \\ 0\ \ 0\ \ 0 & 1 \end{bmatrix};$$
6. Compute the deflected pose using the forward kinematics with the deflected homogeneous transformations.

Given a commanded pose, the tilt, and the force exerted by the end effector, the modified commanded pose is computed as follows:

1. Compute the joint angles, q_{cmd}, associated with the command pose using the inverse kinematics;
2. Compute the commanded homogeneous transformation, ${}^{rvr}T_{cmd}$, using the forward kinematics;
3. Compute the deflected homogeneous transformation, ${}^{rvr}T_d$, using the deflection computation algorithm of described above with q_{cmd} as the joint angles;
4. Compute the modified commanded homogeneous transformation:
$${}^{rvr}\tilde{T}_{cmd} = {}^{rvr}T_{cmd}\, {}^{rvr}T_d^{-1}\, {}^{rvr}T_{cmd} = \begin{bmatrix} {}^{rvr}R_{cmd}\, {}^{rvr}R_d^T\, {}^{rvr}R_{cmd} & {}^{rvr}R_{cmd}\, {}^{rvr}R_d^T ({}^{rvr}p_{cmd} - {}^{rvr}p_d) + {}^{rvr}p_{cmd} \\ 0\ \ 0\ \ 0 & 1 \end{bmatrix}$$

The above transforms the commanded transformation to the modified transformation using the inverse of the computed deflection that is sufficiently accurate for small deflections.

Fault Protection

The IDD FSW monitors the state of the arm and rover prior to and during motion to assess if it is safe to continue or if any faults have occurred. The following types of faults are monitored:

- Trajectory generation error
- Potential collision
- Joint limit violation
- Out-of-envelope error
- Encoder-potentiometer miscompare
- Unexpected contact
- Unexpected motor stall
- Motor over heat
- Motor over current
- Excessive rover tilt
- Excessive change in rover tilt
- Requested preload will exceed structural limits

Motor currents are monitored to prevent excessive joint torques in the event that inadvertent contact of the arm or end effector occurs with the rover or an object in the environment. The current limits are computed based on the pose of the arm at each via point and the temperature. The pose-dependent portion of the current limit is computed using the deflection algorithm described above to get the joint toques necessary to statically hold the arm in position and additional amount to account for dynamic effects.

The temperature-dependent portion of the current limit is represented as the no-load motor current. Each joint was characterized for no-load current over temperature and speed. The no-load current is computed from:
$$i_{nl} = c_0 + c_1 e^{c_2 T} + c_3 \omega\, e^{c_4 T}$$
where
c_i = constants derived by fitting to the data
T = temperature
ω = motor speed.

In addition to the running current limits, the joints require higher current at startup to overcome static friction. They are set higher at startup and then reduced on the fly once motion has begun.

Instrument Placement Behavior

During motion the IDD exhibits different behaviors depending on the operation being performed. The behaviors describe how the IDD responds to changes in conditions of contact sensors and joint motors. The IDD exhibits four basic behaviors during motion that are selectable by the operator:

- Free space – no contact is expected and any sense of contact from the contact switches is considered a fault.
- Guarded – contact by the current instrument on the target is expected and IDD motion stops when contact is detected. If the move is a Cartesian move, the pose is saved for future use by the change tool command that positions another instrument on the same target.
- Retracting – the instrument is removed from the target. In this behavior, contact switches for the selected instrument are masked during the move.
- Preload – the instrument is already in contact with the target during this behavior and the contact switches for the selected instrument are masked during the move. During a preload move, the instrument doesn't actually move since it is already

in contact and the desired force is accomplished using the stiffness of the arm as described above in the deflection compensation algorithm.

Collision Checking

IDD collision checking is performed prior to initiation of motion at each via point along Cartesian and joint-space trajectories. The IDD collision checking software is based on FIDO's collision checking software, described in [8]. Collision checking is performed by determining whether or not a geometric model of the rover arm intersects a geometric model of the rover. These geometric models are based on Oriented Bounding Boxes (OBBs) [9] and Oriented Bounding Prisms (OBPs), and are arranged hierarchically to reduce the total number of object-object intersection tests required to determine if an IDD pose is free of collisions. OBBs and OBPs offer a good trade-off of speed and accuracy: no divisions, transcendental operations, or iterations are required to determine if two OBs or OBPs overlap, which leads to an extremely fast and robust implementation. OBBs and OBPs can tightly and efficiently bound the IDD geometry in a small number of primitives.

The collision checking software allows object and hierarchy definitions to be modified without recompilation so that changes can be made via commands sent to the rover. The IDD and rover are represented geometrically as a collection of OBBs and OBPs attached to the coordinate system of each link. Each OBB/OBP is stored as an IDD collision object structure in a global list.

The current pose of each link is computing using the forward kinematic equations for the IDD, along with the predicted IDD deflection at each joint. If substantial deflection is expected within some links (as opposed to bearing slop at the joints), then the OBPs associated with the links will be expanded to account for the maximum deflected volume of the links. Object poses are defined relative to link coordinates, and the world-space object poses are computed by concatenating the relative pose to the pose of the link with which the object is associated.

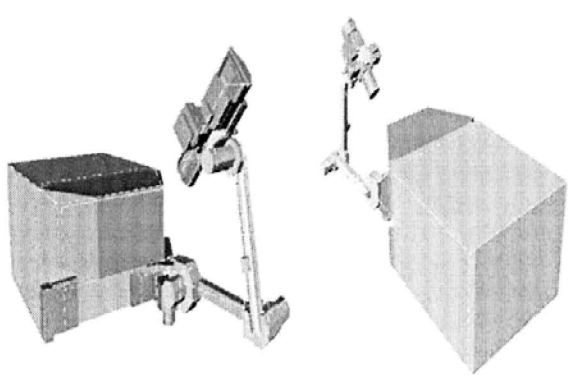

Figure 8: Partial OOB/OBP Models

The MER model is composed of a three-level hierarchy of OBPs and OBBs, with tight-fitting OBBs/OBPs for link geometry at the lowest level being contained within larger, less-accurate OBBs/OBPs at a higher level. The depth of the hierarchy is fixed at compile time. Only those objects that are leaves (i.e. have no child objects) actually represent the rover's geometry; the rest are containers that reduce the total number of object-to-object intersection tests. In addition to the IDD, the rover objects, solar panels, rockers, and front wheels are also modeled as a hierarchical collection of OBBs/OBPs. Figure 8 shows a portion of the OBB/OBP model for the collision checking software. The dashed boxes are container objects, while solid objects are lower level primitives directly representing rover geometry. The hierarchy level of each object is represented by color: yellow is highest, then grey, then blue. Each link has an independent hierarchy of objects.

4. SUB-SYSTEM CALIBRATION

The primary sub-system calibration of the IDD consisted of "learning" the unique set of D-H parameters documented in Table 1, the joint position offsets, and the stiffness parameters described in Section 4. This was accomplished by making use a precision measurement device known as a laser tracker to determine the 3D position of targets mounted to the end of the IDD as the robotic arm was moved throughout its workspace. A total of 2 laser tracker target brackets were mounted to test fixtures attached to the APXS and RAT mounting locations on the IDD turret. Each laser tracker target bracket was capable accepting 2 laser tracker targets. At unique IDD poses, the 3D location of two of the four targets was measured and the joint angles associated with the IDD pose were recorded within the IDD data product. Using the collected data sets, the parameters are computed using the parameter estimation technique that minimizes the least-squared error between the measured 3D position of the laser tracker targets and the computed 3D position of the laser tracker target using the deflected kinematics of the IDD.

For the Spirit rover, the data collection consisted of moving the IDD through a total of 96 poses in the three distinct turret and IDD configurations and measuring the 3D position of two of the four laser tracker targets resulting in a total of 192 data points. The first configuration consisted of the IDD in a level configuration and the just the two laser tracker brackets mounted to the turret. The second configuration had the IDD in a level configuration with two laser tracker brackets mounted to the turret along with mass models mounted to the MB and MI mounting locations of the turret. In this configuration, the total mass of the laser tracker targets and the mass models simulated the full mass and center of mass of the *in situ* instruments as configured on the turret. The third configuration utilized the same turret configuration as the second configuration (laser tracker brackets and mass models) and tilting the IDD and

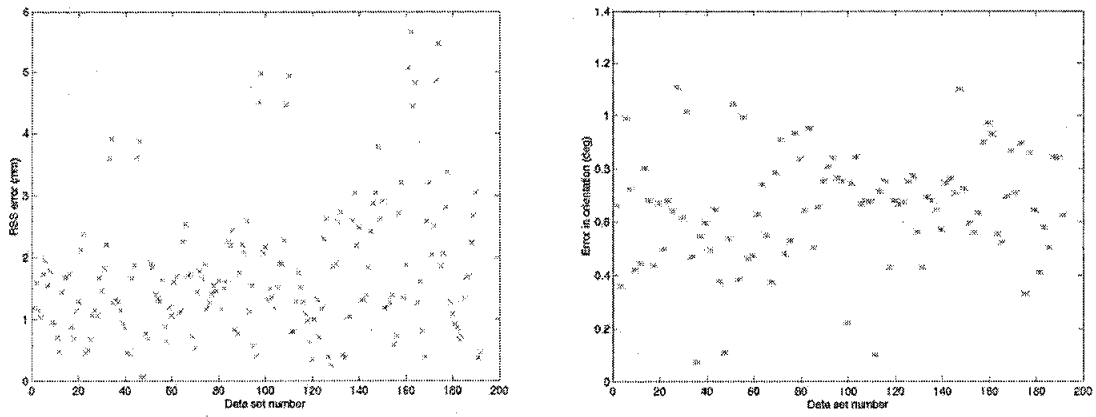

Figure 9: RSS position and orientation error for Spirit's IDD

Parameters	Nominal	Spirit IDD	Opportunity IDD
(a_1, a_2, a_3) meters	(0.062, 0.354, 0.331)	(0.064, 0.353, 0.330)	(0.062, 0.354, 0.330)
(d_1, d_4, d_5) meters	(0.048, -0.099, -0.080)	(0.048, -0.100, -0.077)	(0.048, -0.099, -0.077)
$(\theta_1, \theta_2, \theta_3, \theta_4, \theta_5)$ radians	(0, 0, 0, 0, 0)	(-0.012, 0.004, -0.033, 0.028, -0.016)	(-0.010, 0.004, -0.029, 0.032, -0.039)
Link 1 (k_x, k_y, k_z) N-m/rad	(6106.9, 5892.0, 3922.7)	(6106.9, 5892.0, 3922.7)	(6106.9, 5892.0, 3922.7)
Link 2 (k_x, k_y, k_z) N-m/rad	(1871.5, 5887.2, 2761.9)	(1871.5, 5887.5, 2761.8)	(1871.5, 5887.5, 2761.8)
Link 3 (k_x, k_y, k_z) N-m/rad	(499.2, 780.7, 485.6)	(499.2, 780.7, 485.6)	(499.2, 780.7, 485.6)
Link 4 (k_x, k_y, k_z) N-m/rad	(3367.9, 1227.4, 322.2)	(3367.9, 1227.4, 322.2)	(3367.9, 1227.4, 322.2)
Link 5 (k_x, k_y, k_z) N-m/rad	(1112.5, 45438.0, 1024.7)	(1112.5, 45438.0, 1024.7)	(1112.5, 45438.0, 1024.7)

Table 2: IDD Calibration Parameters

associated ground support hardware by approximately 20 degrees. Finally, a "truth" data set was collected by moving the IDD through a different set of 30 poses in the third configuration. This truth set was not included in the least-squared error estimation process and was used to validate the parameters determined by this estimation process.

The position and orientation error residuals associated with the Spirit IDD training set are shown in Figure 9. The calibrated kinematic and stiffness parameters when compared to the nominal parameters that are derived from the CAD and finite element models of the IDD are shown in Figure 9. The mean root sum squared (RSS) error associated with the Spirit IDD training set is 1.717 mm in position and 0.655 degrees in orientation. The mean plus 3σ RSS error for the Spirit IDD is 4.970 mm in position and 1.276 degrees in orientation. For the truth set, the mean RSS error is 2.081 mm in position and 0.677 degrees in position with the mean plus 3σ RSS error of 5.807 mm in position and 1.347 degrees in orientation. These RSS error number should be compared to the IDD positioning and orientation requirements described in Section 2 which specified a requirement of 5 mm in position and 5 degrees in orientation. Clearly, the Spirit IDD positioning and orientation performance exceeds the stated requirements.

For the Opportunity rover, the IDD calibration data collection process was similar to the Spirit rover with the exception of the inclusion of the third tilted configuration in the calibration data set. The data collection therefore consisted of 60 poses total. The position and orientation residuals associated with the Opportunity IDD training set are similar to the Spirit data shown in Figure 9. The calibrated kinematic and stiffness parameters are also shown in Table 2 along with the Spirit and nominal parameter values. The mean RSS error associated with the Opportunity IDD training set is 1.024 mm in position and 0.452 degrees in orientation with the mean plus 3σ RSS error of 3.220 mm in position and 1.128 degrees in orientation. The truth set data consisted of 30 poses and resulted in a mean RSS error of 1.331 mm in position and 0.482 degrees in orientation with a mean plus 3σ RSS error of 3.560 mm in position and 1.202 degrees in orientation.

It is interesting to note that in Table 2, the parameter estimation process tends to modify the D-H parameters and the joint offset values as opposed to modifying the stiffness parameters. In other words, the majority of the stiffness parameters in Table 2 did not vary from their initial, modeled value while all of the D-H parameters and joint offset values were updated through the least-squared error estimation process. From this result, the underlying

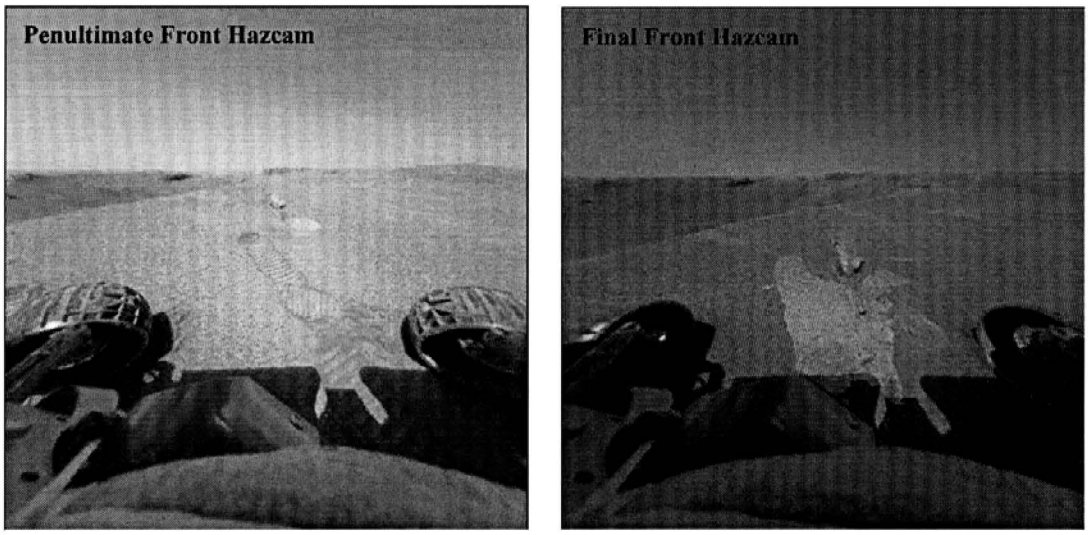

Figure 10: Penulatimate and final front Hazcam images and associated Reachability Map

sensitivity of the parameters as they related to the 3D position of the laser tracker targets mounted to the end of the IDD is assumed be greater for the D-H and joint offset parameters when compared to the stiffness parameters. Finally, it is worth noting that the parameter estimation process described above subsumes any unmodeled effects (joint backlash, workmanship issues such non-orthogonal links, etc) into the parameters that have been modeled. It is not expected that the final parameter sets shown in Table 2 are representative of the real, as-measured IDD, but instead represent the best fit of the parameters to the model that relates IDD joint angles to end-effector or tool position.

In addition to the kinematic and stiffness calibration process, the repeatability of the IDD was measured by moving the robot arm to specific poses within its workspace and measuring the laser tracker targets mounted to the IDD turret. A limited data set was captured for the Spirit IDD and the resulting mean RSS position repeatability is 0.34 mm in position and 0.19 degrees in orientation. The mean plus 3σ RSS position error is 0.42 mm and 0.25 degrees in orientation. A more extensive dataset was collected using the Engineering Model (EM) IDD and, for this arm, the resulting mean RSS position repeatability is 0.31 mm in position and 0.29 degrees in orientation while the mean plus 3σ RSS position error is 1.32 mm and 1.19 degrees in orientation. Recall that the system requirement for repeatability was specified to be 4 mm in position and 3 degrees in orientation. Clearly, the IDD exceeded this performance requirement by almost an order of magnitude for the mean position and orientation repeatability. The repeatability of the IDD turned out to be critical for certain surface operation functions as described in the next section.

Finally, as mentioned previously, the IDD was responsible for placing the in situ instruments on rover-mounted target (magnets and CCT) as well as deploying and stowing to the stow-for-drive position that was tucked under the front of the rover. To accomplish these positioning duties, the standard "teach-repeat" technique where, during ground testing, the desired instrument was precisely positioned relative to the rover-mounted target and the joint angles at this position were recorded. Since these teach points were learned under Earth gravity conditions, the deflection of the turret-mounted instruments will be different during surface operations due to Martian gravity conditions. To account for this difference, the pose of the desired instrument is computed using the taught joint angles and the deflected kinematics described in Section 3. This taught pose is then used during Martian surface operations to command the desired instrument to the desired rover-mounted target. The deflection compensation technique described in Section 3 is utilized to compute the joint angles that achieve the desired end pose. These computed joint angles will certainly be different from the joint angles taught during Earth testing, however, the desired end pose will be the same on Mars as it was on the Earth.

The other related "teach-repeat" position set is associated with deploying the IDD from the stowed position under the rover and stowing it back to this position prior to rover mobility. The IDD deploy and stow operation consists of moving the IDD through a set of mostly single joint moves that maneuver the arm around and into various stow features mounted to the rover. Due to the changes in gravity conditions from when the deploy/stow sequence is taught to the IDD, the individual joint motions were modified by the expected droop of the IDD relative to the stow features when operating the IDD on the Martian surface.

5. SURFACE OPERATIONS HIGHLIGHTS

In this section, the primary process for operating the IDD and associated *in situ* instruments is described along with some representative results from Martian surface operations. The surface operation of the IDD starts with the acquisition of a set of front Hazcam stereo image pairs. Typically, two stereo pairs are acquired with the first designated as the penultimate Hazcam and the second designated as the final Hazcam with 50-80 cm of rover motion separating the two image pairs. Two images are acquired since the entire deployment volume of the IDD as it moves out of its stow position is not visible completely within the final front Hazcam. The penultimate image pair serves as a means to check what is under the rover in the final position and to validate that the deploy volume is clear of any objects that would interfere with the IDD deployment. Representative penultimate and final front Hazcam stereo images from the Opportunity rover outside of Endurance crater are shown in Figure 10.

When the final front Hazcam stereo image pair gets transmitted from the rover to Earth, a data processing pipeline operates on the image pair in order to generate stereo range data relative to the rover reference frame. From this generated range map, a number of products are derived including a surface normal map which is computed by fitting (in a least-squared error sense) a plane to the cloud of range points surrounding a valid point in the stereo range map. From the combined range map and surface normal map, the ability of the IDD to reach out and place each one of the *in situ* instruments on the valid range and surface normal points. This so-called "reachability" map is then used to select targets for science instrument placement activities. The computation of the reachability map includes testing the four major configurations of the IDD (elbow up and wrist up, elbow down and wrist up, elbow up and wrist down, and elbow down and wrist down) as well as predicted collisions between the IDD, the *in situ* instruments, the rover, and the terrain using the collision detection algorithm described in Section 4. A representative reachability map from the Opportunity rover is shown in the left image in Figure 10 and the subsequence placement of the APXS instrument on this rock is shown in Figure 11.

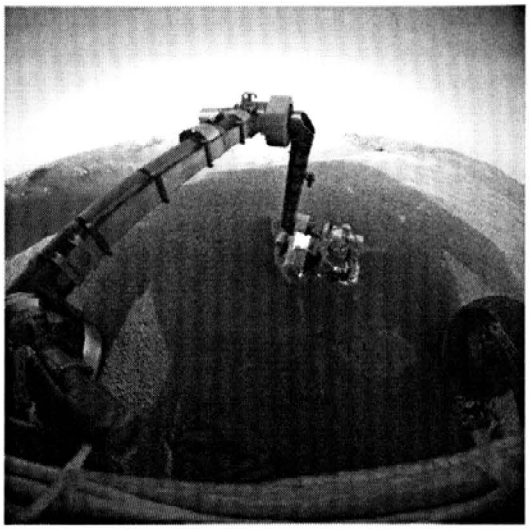

Figure 11: APXS placement

The MER Instrument Positioning System has performed numerous deploy/stow cycles and many *in situ* observations while deployed. A full accounting of the number of deploy/stow cycles and science observations per rover has not been performed, however, a tally was made for the Opportunity rover at the end of its prime mission (90 sols on Mars). By sol 90, the IDD had been deployed and stowed 36 times, acquired 43 APXS measurements, acquired 89 MB spectrometer measurements, acquired 766 MI images, and performed 8 RAT grind activities.

6. CONCLUSIONS

This paper has described in detail the Mars Exploration Rover's Instrument Positioning System and the use of this sub-system to carryout *in situ* operations of the Martian surface and sub-surface. All told, the IDD has served as an exceptional robotic mechanism for performing robust and reliable *in situ* science. The ability to carry out high precision mobile manipulation functions provided by the rover and the IDD has been critical to the understanding of the water processes at both the Spirit and Opportunity landing sites. The Mars Exploration Rover's Instrument Positioning System has paved the way for the use of future robotic devices that advance NASA's capabilities in autonomous manipulation, sample acquisition, and *in situ* science investigations.

REFERENCES

[1] S. W. Squyres, et al., "Athena Mars Rover Science Investigation," *Journal of Geophysical Research, 108*(E12), 8062, doi:10.1029/2003JE002121, 2003.

[2] G. Klingelhöfer, et al., "Athena MIMOS II Mössbauer Spectrometer Investigation," *Journal of Geophysical Research, 108*(E12), 8067, doi:10.1029/2003JE002138, 2003.

[3]R. Rieder, et al., "The New Athena Alpha Particle X-ray Spectrometer for the Mars Exploration Rovers, *Journal of Geophysical Research, 108*(E12), 8066, doi:10.1029/2003JE002150, 2003.

[4] K. E. Herkenhoff, et al., Athena Microscopic Imager Investigation, *Journal of Geophysical Research, 108*(E12), 8065, doi:10.1029/2003JE002076, 2003.

[5] S. P. Gorevan, et al., "Rock Abrasion Tool: Mars Exploration Rover Mission," *Journal of Geophysical Research, 108*(E12), 8068, doi:10.1029/2003JE002061, 2003.

[6] R. Fleischner, "Concurrent Actuator Development for the Mars Exploration Rover Instrument Deployment Device," *Proceedings of the 10th European Space Mechanisms and Tribology Symposium*, San Sebastian, Spain, September 2003.

[7] M. W. Spong and M. Vidyasagar, *Robot Dynamics and Control*, John Wiley and Sons, Inc., New York, 1989.

[8] C. Leger, "Efficient Sensor/Model Based On-Line Collision Detection for Planetary Manipulators," *Proceedings of the 2002 IEEE International Conference on Robotics and Automation*, pp. 1697-1703, May 2002.

[9] S. Gottschalk, M. C. Lin and D. Manoch, *OBB-Tree: A hierarchical Structure for Rapid Interference Detection.* Technical Report TR96-013, Department of Computer Science, University of North Carolina, Chapel Hill, 1996.

BIOGRAPHY

Eric T. Baumgartner is a . . . (to be completed in final version)

Robert G. Bonitz is a . . . (to be completed in final version)

Lori R. Shiraishi is a . . . (to be completed in final version)

Joseph P. Melko is a . . . (to be completed in final version)

P. Chris Leger is a . . . (to be completed in final version)